Chemosphere 117 (2014) 256–261

Contents lists available at ScienceDirect

Chemosphere

journal homepage: www.elsevier.com/locate/chemosphere

Solar photo-Fenton using peroxymonosulfate for organic micropollutants removal from domestic wastewater: Comparison with heterogeneous TiO_2 photocatalysis

Moussa Mahdi Ahmed [a,*], Monica Brienza [b], Vincent Goetz [b], Serge Chiron [a]

[a] UMR HydroSciences 5569, Montpellier Université, 15 Avenue Ch. Flahault, 34093 Montpellier cedex 5, France
[b] PROMES-CNRS, UPR 8521, Tecnosud, Rambla de la Thermodynamique, 66100 Perpignan, France

HIGHLIGHTS

- UV–Vis/PMS/Fe(II) was ten times faster than UV–Vis/TiO_2 for pesticide and pharmaceutical removal.
- Higher TOC abatement was obtained in UV–Vis/PMS/Fe(II) system.
- Sulfate radical reactivity was responsible for mesotrione degradation kinetic enhancement.
- A specific sulfate radical transformation route involved one electron oxidation reactions.
- This selective and additional pathway accounted for enhanced mesotrione removal in wastewater.

ARTICLE INFO

Article history:
Received 19 May 2014
Received in revised form 15 July 2014
Accepted 15 July 2014
Available online 8 August 2014

Handling Editor: E. Brillas

Keywords:
Sulfate radical
Wastewater
Solar photo-Fenton
Mesotrione
Transformation pathways

ABSTRACT

This work aims at decontaminating biologically treated domestic wastewater effluents from organic micropollutants by sulfate radical based ($SO_4^{\cdot-}$) homogeneous photo-Fenton involving peroxymonosulfate as an oxidant, ferrous iron (Fe(II)) as a catalyst and simulated solar irradiation as a light source. This oxidative system was evaluated by using several probe compounds belonging to pesticides (bifenthrin, mesotrione and clothianidin) and pharmaceuticals (diclofenac, sulfamethoxazole and carbamazepine) classes and its kinetic efficiency was compared to that to the well known UV–Vis/TiO_2 heterogeneous photocatalysis. Except for carbamazepine, apparent kinetic rate constants were always 10 times higher in PMS/Fe(II)/UV–Vis than in TiO_2/UV–Vis system and more than 70% of total organic carbon abatement was reached in less than one hour treatment. Hydroxyl radical ($^{\cdot}OH$) and $SO_4^{\cdot-}$ reactivity was investigated using mesotrione as a probe compound through by-products identification by liquid chromatography-high resolution-mass spectrometry and transformation pathways elucidation. In addition to two $^{\cdot}OH$ based transformation pathways, a specific $SO_4^{\cdot-}$ transformation pathway which first involved degradation through one electron transfer oxidation processes followed by decarboxylation were probably responsible for mesotrione degradation kinetic improvement upon UV–Vis/PMS/Fe(II) system in comparison to UVVis/TiO_2 system.

1. Introduction

Domestic wastewater treatment plants (WWTPs) effluent reuse has emerged as one of the most viable approaches to alleviate water stress (Norton-Brandao et al., 2013). However, its wider acceptance is hampered in part by the presence of organic micropollutants such as pharmaceutical and pesticide residues, which are slightly transformed or even unchanged during current biological water treatment (Jelic et al., 2011). The occurrence of pesticides in domestic WWTPs effluents has been less investigated than pharmaceuticals but has emerged to be a relevant issue in terms of diversity of identified compounds and concentrations (Campo et al., 2013), herbicides (Parry and Young, 2013), and insecticides (Köck-Schulmeyer et al., 2013) being the most often detected compounds. Advanced oxidation processes (AOPs) have turned out to be one of the promising and competitive technologies for the abatement of various bio-recalcitrant organic

* Corresponding author. Tel.: +33 (0) 4 11 75 94 68; fax: +33 (0) 4 11 75 94 61.
E-mail address: moussa.mahdi@chemist.com (M.M. Ahmed).

http://dx.doi.org/10.1016/j.chemosphere.2014.07.046
0045-6535/

micropollutants in biologically treated domestic wastewaters treatment (Pablos et al., 2013). The AOPs strength relies on the promotion of the highly oxidative hydroxyl radical ($HO^{\cdot}$) by various combinations such as UV/H_2O_2, UV/O_3, UV/TiO_2 and Fenton/photo-Fenton technologies. More recently, the oxidation of organic compounds by persulfate (PDS = $S_2O_8^{2-}$) or peroxymonosulfate (PMS = HSO_5^-) has been studied as an alternative to conventional $HO^{\cdot}$ based AOPs. In such systems, PDS and PMS decompose to the sulfate radical ($SO_4^{\cdot-}$) which is a strong oxidant with a redox potential of 2.5–3.1 V. Transition metals such as Ag^+ or Co^{2+} were found to be active in initiating $SO_4^{\cdot-}$ generation from PDS/PMS for pollutant degradation (Anipsitakis and Dionysiou, 2004; Mahdi Ahmed et al., 2012) but naturally occurring metal (i.e., iron (Vicente et al., 2011)) or ferrites (Zhang et al., 2013) have also been identified to be able to activate PDS or PMS for the degradation of contaminants. Recently, combining UV-C irradiation (Ali Khan et al., 2013; Mahdi Ahmed and Chiron, 2014a) or simulated solar irradiation (Mahdi Ahmed and Chiron, 2014b) with free Fe(II) resulted in an increase in efficiency for UV–Vis/PDS/Fe(II) and UV–Vis/PMS/Fe(II) oxidation systems. This combination might be beneficial for devising economical feasible remediation strategies for removing recalcitrant organic micropollutants such as pharmaceuticals and pesticides. Even though the superiority of UV–Vis/PMS/Fe(II) over UV–Vis/H_2O_2/Fe(II) for organic micropollutants removal from domestic wastewater has been rationalized by the higher selectivity in reactivity of $SO_4^{\cdot-}$ over $HO^{\cdot}$ in organic-rich matrices, little effort has been devoted to compare UV–Vis/PMS/Fe(II) to UV–Vis/TiO_2 oxidative system. This will be the main contribution of this work and the specific aims are the followings:

(i) To compare UV–Vis/PMS/Fe(II) with UV–Vis/TiO_2 systems on the basis of kinetic parameters and using six different compounds belonging to the pesticide (bifenthrin (BFN), clothianidin (CLT) and mesotrione (MTN)) and the pharmaceutical (carbamazepine (CBZ), diclofenac (DCF) and sulfamethoxazole (SMX)) classes and encompassing a large variety of chemical structures and physico-chemical properties (see Fig. 1).

(ii) To better understand sulfate reactivity in aqueous media using mesotrione as a probe compound by means of the elucidation of transformation products (TPs) and transformation pathways in an attempt to account for kinetic results.

2. Material and methods

2.1. Chemicals

Analytical grade CLT; BFN, MTN, CBZ, DCF and SMX standards, iron(II) sulfate ($FeSO_4{\cdot}7H_2O$, 99%), peroxymonosulfate (available as a triple potassium salt with the commercial name of Oxone, 2 $KHSO_5{\cdot}KHSO_4{\cdot}K_2SO_4$) were purchased from Sigma Aldrich (St Quentin Fallavier, France). TiO_2 (Aeroxide) was a gift from Evonik (Germany). Sodium nitrite ($NaNO_2$, 98%), monosodium phosphate (NaH_2PO_4, 98%) and disodium phosphate (Na_2HPO_4, 98%) salts were purchased from VWR (Fontenay-sous-Bois, France). Methanol (LC grade) and acetonitrile (LC grade) were purchased from Merck (Darmstadt, Germany). All chemicals were used as received without further purification. All aqueous solutions were prepared with UHQ milliQ water (Millipore, Bedford, USA).

2.2. Degradation experiments

The irradiation experiments were carried out in a Solarbox (CO.FO. MEGRA, Milan), where stirred cylindrical closed cells (40 mm i.d.; 25 mm high) made of Pyrex glass were placed. A 1500 W Xenon lamp source, equipped with a 290 nm cut-off fihigh was used to simulate solar irradiation. The photoreactor was water cooled so that the temperature never exceeded 25 °C during irradiation experiments and consequently, heat activation of PMS could be neglected. The total photonic flux in the cell has been kept constant for all the experiments at 7.9×10^{-6} E min^{-1}. Typical experiments included 50 μM of selected contaminant aqueous solution followed by the addition of adequate volume of PMS and Fe(II) from 0.1 M aqueous stock solutions or by addition of 0.5 g L^{-1} TiO_2. pH was set at 3 with H_2SO_4 (1 M) in case of PMS/Fe(II)/UV–Vis system and at pH 7.8 in case of TiO_2/UV–Vis system using a 10 mM phosphate buffer. Wastewater was sampled from a WWTP effluent involving activated sludge and with the following characteristics: pH = 8.4; conductivity = 919 μS cm^{-1}; [TOC] = 50 ± 1.1 mg L^{-1}; [Cl^-] = 71 ± 0.1 mg L^{-1}; [Br^-] = 0.3 ± 0.05 mg L^{-1}; [NO_2^-] = 0.5 ± 0.1 mg L^{-1}; [NO_3^-] = 7.1 ± 0.2 mg L^{-1}; [HCO_3^-] = 22 ± 2 mg L^{-1}; [Ca^{2+}] = 50 ± 3 mg L^{-1}; [Na^+] = 12 ± 2 mg L^{-1}; [K^+] = 1.5 ± 0.2 mg L^{-1}. Aliquots of 5 mL and 1 mL were sampled at selected time intervals for TOC and LC analysis, respectively using sodium nitrite and methanol, respectively for reaction quenching.

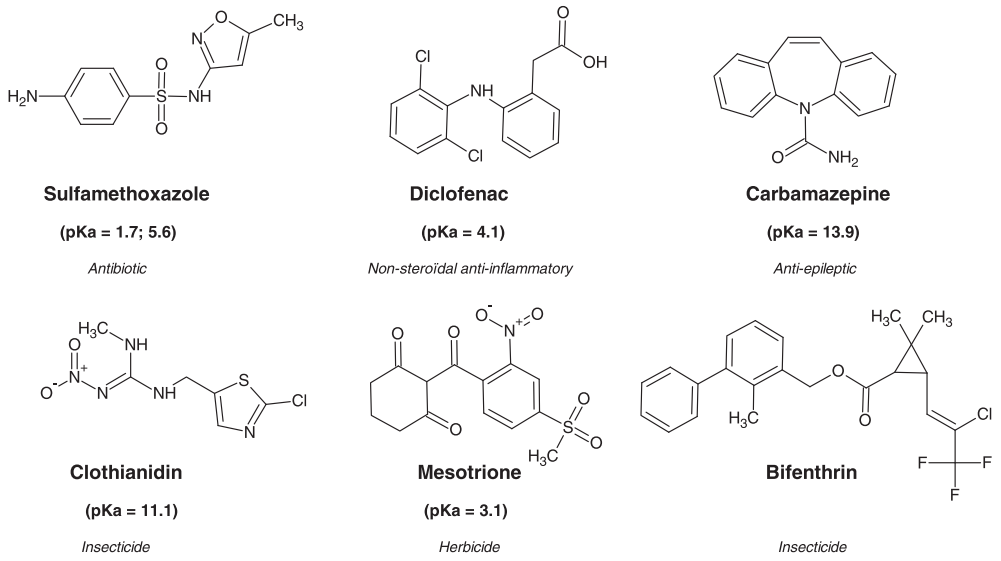

Fig. 1. Chemical structures of investigated pesticide and pharmaceutical compounds.

The experiments were conducted in triplicate to ensure consistency of the results and each kinetic point represents an average of three experiments. All kinetics were in agreement with a pseudo-first order kinetic model and apparent kinetic rate constant (k_{app}) was determined accordingly.

2.3. Analytical methods

Contaminant concentration evolution was followed by HPLC–UV (Ultimate 300, Dionex) equipped with a UV–Vis detector and an Agilent Zorbax C8 column (150 mm × 3.0 mm i.d., 3.5 μm particle size). Analytes were separated with a mixture of methanol:water (40:60, v/v) at a flow rate of 0.4 mL min^{-1} in the isocratic mode of elution with a detection at λ = 220 nm. Total organic carbon (TOC) was measured using a Shimadzu-5050A TOC analyzer. Transformation products (TPs) were detected by using liquid chromatography–electrospray – orbitrap mass spectrometry (Exactive Plus Orbitrap, ThermoScientific) using an electrospray interface in the negative mode of ionization. Separation was done by a HPLC system (Accelera 1250 pump, ThermoScientific) equipped with a Betabasic C-18 analytical column (150 mm × 2.1 mm i.d., 3.5 μm particle size) at a flow rate of 0.2 mL min^{-1}. The mobile phase consisted of binary mixture of solvent A (0.1% formic acid – water) and B (acetonitrile). The gradient was operated from 10% to 30% A for 10 min, from 30% to 90% for 5 min, kept at 100% for 5 min and then back to initial conditions in 5 min. Operating conditions were the followings: electrospray voltage, 4.0 kV; sheath gas, 35 arbitrary units; auxiliary gas, 10 arbitrary units; tube lens, 70 V; skimmer, 16 V and capillary voltage, 65 V. The heater in the source was set to 200 °C and the heated capillary in the mass spectrometer was operated at 300 °C. Full scan analysis was performed in the 100–500 m/z range in order to elucidate TPs structures on the basis of their accurate mass measurement which allowed for empirical formula to be calculated with an elemental composition calculator tool. The low errors in full scan MS obtained (<5 mg L^{-1}) allowed for the high grade of confidence in the assignation of the elemental composition.

3. Results and discussion

3.1. Kinetic studies and comparison between PMS/Fe(II)/UV–Vis and TiO_2/UV–Vis systems

The first aim of this work was to find out optimized conditions to operate the PMS/Fe(II)/UV–Vis and the TiO_2/UV–Vis systems and reported in Table 1 by varying different operating parameters in order to be able to compare them. PMS has been selected in this study because it is more easily activated than PDS by transition metals including Fe(II). In PMS/Fe(II)/UV–Vis system, an acidic pH close to 3 was selected mainly due to the catalyst precipitation at higher pH value. k_{app} reached optimum values when using a PMS:Fe(II) molar ratio of 2:1 as previously reported (Mahdi Ahmed and Chiron, 2014b). In the TiO_2/UV–Vis system, the pH was maintained near the neutrality (7.8) and optimized k_{app} values were obtained with a TiO_2 concentration of 0.5 g L^{-1}. In dark conditions, no loss of investigated compounds was recorded due to direct oxidation by PMS. In contrast, there was an overlap of absorption of compounds and the Xenon lamp emission which consequently led to the degradation of all compounds when solutions were irradiated. However, direct/indirect photolysis was responsible for less than 15% losses of the selected compounds. UV–Vis based AOPs significantly increased the investigated compound removal efficiency in wastewater, whatever the oxidative system used (see Table 1). The most effective process was UV–Vis/PMS/Fe(II) followed by UV–Vis/TiO_2. k_{app} values were always 10 times higher in UV–Vis/PMS/Fe(II) system than in TiO_2 system except for CBZ for which k_{app} was less than seven fold higher than with $HO^{\cdot}$ because this was the only compound which reacted by electron transfer to C—C double bond and not to nitrogen atom (Mahdi Ahmed and Chiron, 2014b). All investigated compounds were totally eliminated within 30 min in UV–Vis/PMS/Fe(II) system. Likely mechanisms to account for higher efficiency of the UV–Vis/PMS/Fe(II) system might be (i) the formation of an inner-sphere complex between Fe(II) and PMS (i.e., a iron(II)-peroxide complex) similarly to those reported with H_2O_2 followed by a photoinduced electron transfer between Fe(II) and PMS enhancing $SO_4^{\cdot-}$ generation and (ii) the PMS activation by several inorganic species such as HCO_3^- and Cl^- (Yuan et al., 2011). At pH 3, chloride ions might play a role in PMS decomposition but only at higher concentration levels (chloride/oxidant molar ratio >10/1) than those found in investigated wastewater (71 mg L^{-1}) (Mahdi Ahmed and Chiron, 2014a). Consequently, observed differences in kinetic patterns between both AOPs could arise from differences between $SO_4^{\cdot-}$ and $HO^{\cdot}$ reactivity in aqueous media (see Section 3.2). Finally, when PMS was added in the TiO_2/UV–Vis system as an electron acceptor, the increase in efficiency was limited probably because the recombination process between holes and electrons was still significant and even though $SO_4^{\cdot-}$ was probably generated (results not shown) (Kitsiou et al., 2009).

TOC evolution was also investigated in distilled water and the results are reported in Fig. 2a and b for PMS/Fe(II)/UV–Vis and TiO_2/UV–Vis, respectively. For homogeneous oxidation the pH was not maintained while for TiO_2 oxidation phosphate buffer was added in distilled water. Less than 50% of TOC abatement

Table 1
Apparent kinetic rate constants (k_{app}) corresponding to the degradation of six pesticide or pharmaceutical compounds under different oxidative systems in biologically treated wastewater effluent.

Compound	Direct photolysis[b] k_{app} ($\times 10^{-2}$ min^{-1})	PMS (mM)[a]	Fe (mM)[a]	k_{app} ($\times 10^{-2}$ min^{-1})	TiO_2 (g L^{-1})[b]	k_{app} ($\times 10^{-2}$ min^{-1})
CLT	–	0.025	0.1	2.1 ± 0.6	0.05	0.18 ± 0.04
CLT	–	0.05	0.1	8.64 ± 0.35	0.1	0.34 ± 0.1
CLT	–	0.1	0.1	19.8 ± 0.14	0.5	1.2 ± 0.09
CLT	–	0.2	0.1	29.54 ± 0.08	1	1.35 ± 0.03
CLT	–	0.3	0.1	25.67 ± 0.75	1.5	1.24 ± 0.08
CLT	–	0.5	0.1	22.48 ± 0.8	2	1.30 ± 0.09
CBZ	0.043 ± 0.2	0.2	0.1	18.69 ± 0.03	0.5	2.96 ± 0.01
DCF	0.68 ± 0.09	0.2	0.1	58.19 ± 0.4	0.5	3.65 ± 0.06
SMX	0.37 ± 0.09	0.2	0.1	54.12 ± 0.1	0.5	3.12 ± 0.02
CLT	0.18 ± 0.07	0.2	0.1	29.54 ± 0.1	0.5	1.20 ± 0.09
MTN	0.10 ± 0.04	0.2	0.1	21.32 ± 0.08	0.5	1.45 ± 0.07
BFT	0.07 ± 0.09	0.2	0.1	28.65 ± 0.06	0.5	1.65 ± 0.08

[a] pH = 3.
[b] pH = 7.8.

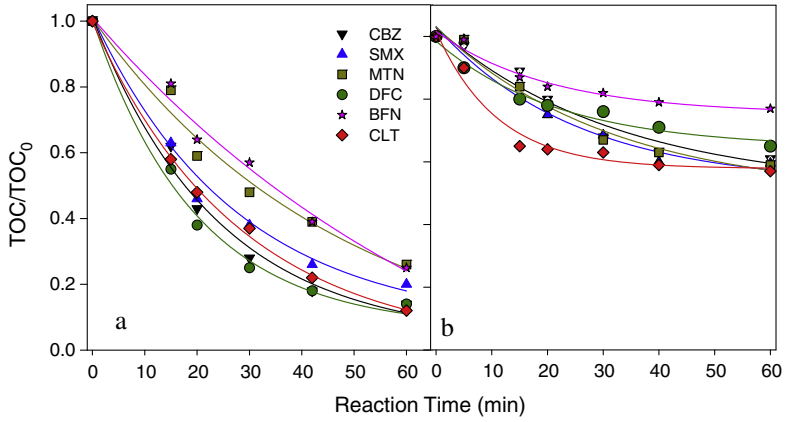

Fig. 2. TOC abatement in distilled water under (a) UV–Vis/PMS/Fe(II) and (b) UV–Vis/TiO_2 oxidative system. Conditions: [compound] = 50 μM, [PMS] = 2 mM, [Fe(II)] = 1 mM, pH 3, [TiO_2] = 0.5 g L^{-1} and pH 7.8.

was obtained in TiO_2/UV–Vis for all investigated compounds, while more than 70% of TOC abatement was reached within the same treatment time in the PMS/Fe(II)/UV–Vis system. A higher efficiency in mineralization rate in this latter system was probably due to the simultaneous generation of $SO_4^{\cdot-}$ and HO· radicals. This latter point will be investigated in the following part.

3.2. Mesotrione transformation pathways elucidation upon PMS/Fe(II)/UV–Vis system

According to oxidizing species generated in AOPs (HO·, $SO_4^{\cdot-}$), different transformation pathways of contaminants has to be expected due to differences in reactivity of each radical specie which might account for differences observed in kinetic patterns. To check for this assumption, MTN has been selected as a probe compound in this work because $SO_4^{\cdot-}$ has proved to be effective in removing nitrogen-rich compounds such as most of the pharmaceuticals (Rickman and Mezyk, 2010; Ji et al., 2014) and carboxylic acid rich compounds such as perfluorocarboxilic acids through decarboxylation processes (Hori et al., 2005) but less is known with sulfate reactivity concerning contaminants lacking such moieties or containing fully oxidized nitrogen atom such as nitro derivatives which react slowly with second order kinetic rate constant values (k_{abs}) < 10^{-6} M^{-1} s^{-1}) with $SO_4^{\cdot-}$ (Neta et al., 1988). In addition, mesotrione TPs have been already identified under direct/indirect photolysis (Ter Halle and Richard, 2006), and under HO· based AOPs such as Fenton and TiO_2 processes (Bensalah et al., 2011; Jović et al., 2013) which might facilitate TPs identification under UV–Vis/PMS/Fe(II). In this study, transformation pathways have been investigated under UV–Vis/TiO_2, and UV–Vis/PMS/Fe(II) oxidative processes. In the UV–Vis/TiO_2 system only five TPs have been detected, while in the UV–Vis/PMS/Fe(II) one, up to ten TPs were detected and identified by LC-HR/MS. Retention times, *m*/*z* ratios, empirical formula together with their calculated and experimental *m*/*z* values of the deprotonated molecular ion are collected in Table 2 for both oxidative systems while, Fig. 3 represents a typical Total Ion Chromatogram (TIC) obtained after 15 min UV–Vis/PMS/Fe(II) treatment time. TPs structures were elucidated on the basis of their accurate mass measurement which allowed for empirical formula to be calculated with an elemental composition calculator tool. The low errors obtained (<4 mg L^{-1}) allowed for a high grade of confidence in the assignation of the elemental composition.

To the best of our knowledge, this is the first time that transformation of MTN under UV–Vis/PMS/Fe(II) has been investigated. A view of MTN transformation pathways under UV–Vis/PMS/Fe(II) is provided in Fig. 4. Most of the TPs have been already identified in previous studies dealing with other oxidative treatments (Jović et al., 2013) or biodegradation (Durand et al., 2006) and a detailed report of MS data interpretation was therefore omitted. Three transformation pathways were proposed taking into account that in the UV–Vis/PMS/Fe(II) system, HO· and $SO_4^{\cdot-}$ are simultaneously generated. In the first one which is a major transformation pathway, keto-enol tautomerism may play a major role because, due to the enol-ketone equilibrium, C2 (see numbering in Fig. 4) is a highly nucleophilic position prone to HO· attacks leading to **P5.** This was also a dominant mechanism in the UV–Vis/TiO_2 system. Further oxidation of **P5** led to the formation of 2-nitro-4-methylsulfonylbenzoic acid (**P3**) which was converted into 2-nitro-4-methylsulfonylphenol (**P9**) by substitution of the carboxylic group

Table 2
Retention time (RT), empirical formula together with their calculated and experimental *m*/*z* values of the deprotonated molecular ions $[M-H]^-$ of detected MTN transformation products (TPs) upon UV–Vis/PMS/Fe(II) and UV–Vis/TiO_2 oxidative processes.

TPs	RT (min)	Formula	DBE	Theoretical mass	Experimental mass	Mass error (Δ mg L^{-1})	TiO_2	PMS/Fe (II)
P1	2.1	$C_6H_7O_5$	3.5	159.0288	159.0291	2.1	X	X
P2	2.6	$C_5H_7O_4$	2.5	131.0339	131.0337	−1.2	X	X
P3	2.9	$C_8H_6NO_6S$	6.5	243.9910	243.9913	1.2	X	X
P4	4.4	$C_{10}H_8NO_7S$	7.5	286.0016	286.0028	4.3		X
P5	6.6	$C_{14}H_{12}NO_8S$	9.5	354.0278	354.0283	1.8	X	X
P6	6.9	$C_{14}H_{12}NO_9S$	9.5	370.0241	370.0241	3.7		X
P7	7.5	$C_{14}H_{14}NO_8S$	8.5	356.0435	356.0437	1.2		X
P8	7.8	$C_{13}H_{14}NO_8S$	7.5	328.0485	328.0498	3.7		X
P9	9.8	$C_7H_6NO_5S$	5.5	215.9961	215.9970	3.9	X	X
P10	10.2	$C_{14}H_{12}NO_8S$	9.5	354.0278	354.0298	3.7		X
MTN	11.4	$C_{14}H_{12}NO_7S$	9.5	338.0329	338.0333	1.3	X	X

DBE: Double bond equivalent.

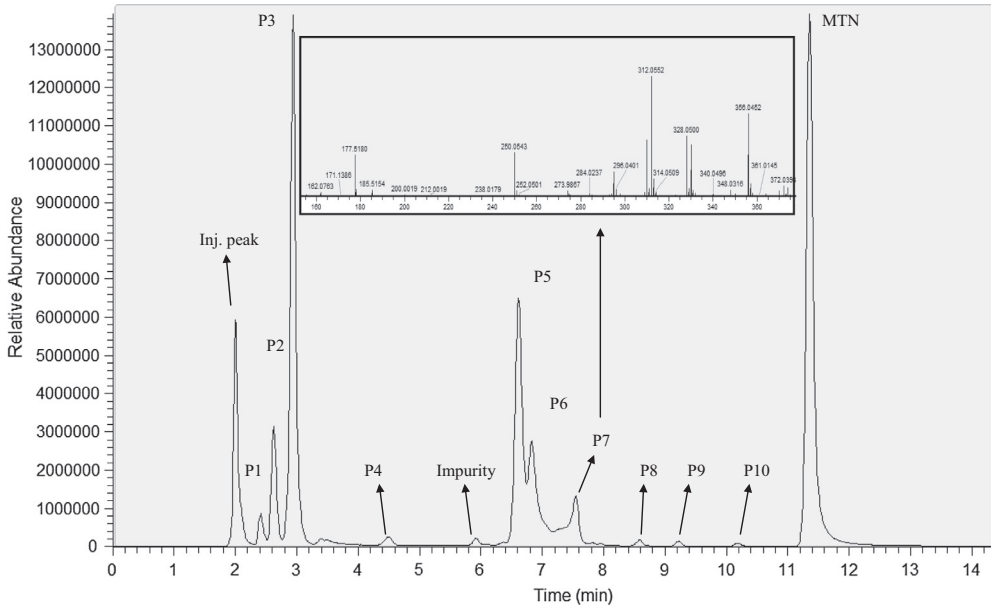

Fig. 3. Total Ion Chromatogram (TIC) chromatogram corresponding to mesotrione degradation after 15 min UV–Vis/PMS/Fe(II) treatment at pH 3. Insert: mass spectrum of transformation product P7 with CID energy = 10 eV.

by a hydroxyl group. Concomitantly, the cyclohexane part of MTN molecule underwent oxidative ring opening and quickly transformed into two major aliphatic carboxylic acids: Glutaric acid (**P2**) and 3-hydroxy-2-hexenoic diacid (**P1**). The second transformation pathway, which is a minor one, involved hydroxylation steps of the aromatic ring. MTN contains a strong electron withdrawing group (–NO_2) and the first hydroxylation step logically occurred at C_{13} position (**P10**) followed by C_{12} position (**P6**). Hydroxylation through $SO_4^{\bullet-}$ reactivity cannot be ruled out because $SO_4^{\bullet-}$ mediated aromatic ring attack can also lead to the formation of the hydroxycyclohexadienyl radical ($C_6H_6O^{\bullet}$) via one electron transfer reaction between phenol and $SO_4^{\bullet-}$. This radical evolves to hydroxylated radical intermediates followed by the formation of more stable degradation products upon their further reaction with oxygen including catechol and hydroquinone (Olmez-Hanci and Arslan-Alaton, 2013). This pathway was not observed in case of UV–Vis/TiO_2 treatment, probably because P**10** and P**6** were generated in too low amounts to be detected. The third pathway, which is a major pathway, is probably specifically related to $SO_4^{\bullet-}$ reactivity because it was never detected upon UV–Vis/TiO_2 oxidation. Due to its high acidity (p*K*a 3.1), the enol groups of MTN are partially dissociated at pH 3. Enolate probably easily underwent a one electron oxidation to give rise to a phenoxyl like radical. This radical might evolve into 5,7-diketo-7-(2-nitro-4-methylsulfonylphenyl)-heptanoic acid (**P7**) through C_2–C_3 double bond oxidation. Mass spectrum of this key intermediate is presented in the insert of

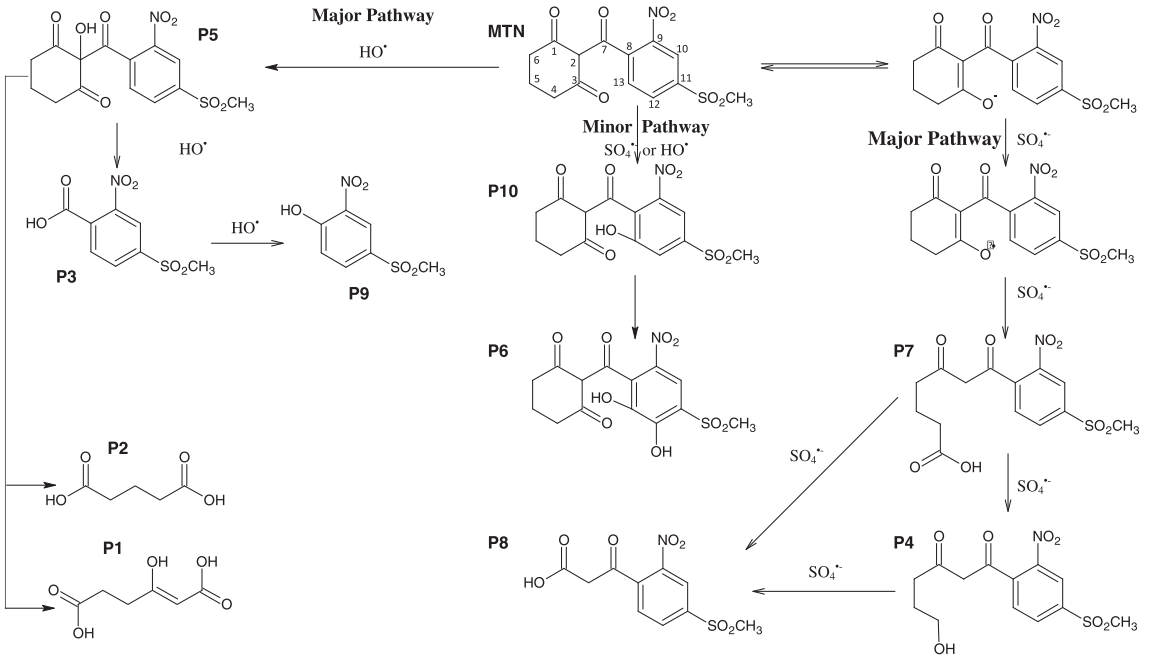

Fig. 4. Proposed mesotrione transformation pathways upon UV–Vis/PMS/Fe(II) oxidative system.

Fig. 3 and it is characterized by a pseudo molecular ion $[M-H]^-$ at m/z = 356.0442 and a fragment ion at m/z = 312.0552 as base peak, corresponding to m/z = 43.989 losses characteristic of CO_2 losses. **P7** has been already detected under direct photolysis (Ter Halle and Richard, 2006) probably due to a photohydrolysis of the C_2–C_3 bond. Then, **P7** underwent a decarboxylation step as reported for others aliphatic acid (Karpel Vel Leitner and Criquet, 2009) leading to the formation of a primary alcohol (**P4**) or was further oxidized into 1,3-diketo-3-(2-nitro-4-methylsulfonylphenyl)butanoic acid (**P8).** This additional degradation route in comparison to UV–Vis/TiO_2 was in part responsible for the enhancement of MTN degradation kinetics upon UV–Vis/PMS/Fe (II). In addition, $SO_4^{\cdot-}$ might react more selectively than $HO^{\cdot}$ against MTN in wastewater due to a one electron oxidation mechanism as a starting point of MTN transformation. This mechanism is probably poorly scavenged by dissolved organic matter (DOM) because, even though DOM is rich in phenol or enol moieties, these latter are not dissociated and electron abstraction by $SO_4^{\cdot-}$ is not a favored mechanism with phenol with respect to phenolate ion. In contrast, $HO^{\cdot}$ reactivity is heavily scavenged by DOM because this radical mainly reacts through addition on unsaturated C–C bonds. Consequently, the higher selectivity of the $SO_4^{\cdot-}$ route also contributed to the MTN degradation kinetics enhancement in wastewater.

4. Conclusions

PMS/Fe(II)/UV–Vis advanced oxidation system using simulated solar irradiation has demonstrated better kinetic performances over TiO_2/UV–Vis system for six organic micropollutants removal in WWTP effluents mainly due to the higher selectivity in reactivity of $SO_4^{\cdot-}$ with respect to $HO^{\cdot}$ in organic rich matrices A molar ratio PMS:Fe(II) of 2:1 was found to be optimum for a full mineralization of investigated compounds in 30 min. This study has revealed the usefulness for a better understanding of $SO_4^{\cdot-}$ reactivity in aqueous media for kinetic results interpretations. When dealing with $SO_4^{\cdot-}$ radical, specific and additional routes of degradation routes are involved as demonstrated in this work with the particular case of MTN but also endorsing previous results obtained with nitrogen-rich pharmaceuticals (Mahdi Ahmed and Chiron, 2014b). This specific route of degradation is related to one electron transfer oxidation processes as starting point for contaminant degradation upon $SO_4^{\cdot-}$ which are less scavenged in complex organic matrices than radical addition on unsaturated C–C bond processes, typical of $HO^{\cdot}$ reactivity. The possibility to use solar irradiation to activate PMS into radical species in the PMS/Fe(II)/UV–Vis advanced oxidation system probably opens new economical feasible remediation strategies for WWTPs effluent tertiary treatment before wastewater reuse in irrigation for instance. Further works will aim to scaling up the process.

Acknowledgements

This study was funded by the European ENPI-CBC-MED program (NANOWAT project, ref. I-B/2.1/049). This research benefited from the support of the ≪ Chair VEOLIA ENVIRONNEMENT – HydroSciences: Risk analysis relating to emerging contaminants in water bodies ≫.

References

Ali Khan, J., He, X., Khan, H., Shah, N., Dionysiou, D., 2013. Oxidative degradation of atrazine in aqueous solution by UV/H_2O_2/Fe^{2+}, UV/$S_2O_8^{2-}$/Fe^{2+} and UV/HSO_5^-/Fe^{2+} processes: a comparative study. Chem. Eng. J. 218, 376–383.
Anipsitakis, G.P., Dionysiou, D., 2004. Transition metal/UV-based advanced oxidation technologies for water decontamination. Appl. Catal. B: Environ. 254, 55–163.
Bensalah, N., Khodary, A., Abdel-Wahab, A., 2011. Kinetic and mechanistic investigations of mesotrione degradation in aqueous medium by Fenton process. J. Hazard. Mater. 189, 479–485.
Campo, J., Masia, A., Blasco, C., Pico, Y., 2013. Occurrence and removal efficiency of pesticides in sewage treatment plants of four Mediterranean River Basins. J. Hazard. Mater. 263, 146–157.
Durand, S., Legeret, B., Martin, A.-S., Sancelme, M., Delart, A.-M., Besse-Hogan, P., Combourieu, B., 2006. Biotransformation of the triketone herbicide mesotrione by a Bacillus strain. Metabolite profiling using liquid chromatography/electrospray ionization quadrupole time-of-flight mass spectrometry. Rapid Commun. Mass Spectrom. 20, 2603–2613.
Hori, H., Yamamoto, A., Hayakawa, E., Taniyasu, S., Yamashita, N., Kutsuna, S., 2005. Efficient decomposition of environmentally persistent perfluorocarboxylic acids by use of persulfate as a photochemical oxidant. Environ. Sci. Technol. 39, 2383–2388.
Jelic, A., Gros, M., Ginebreda, A., Cespedes-Sánchez, R., Ventura, F., Petrovic, M., Barcelo, D., 2011. Occurrence partition and removal of pharmaceuticals in sewage water and sludge during wastewater treatment. Water Res. 45, 1165–1176.
Ji, Y., Ferronato, C., Salvador, A., Yanga, X., Chovelon, J.-M., 2014. Degradation of ciprofloxacin and sulfamethoxazole by ferrous-activated persulfate: implications for remediation of groundwater contaminated by antibiotics. Sci. Total Environ. 472, 800–808.
Jović, M., Manojlović, D., Stanković, D., Dojčinović, B., Obradović, B., Gašić, U., Roglić, G., 2013. Degradation of triketone herbicides, mesotrione and sulcotrione, using advanced oxidation processes. J. Hazard. Mater. 260, 1092–1099.
Karpel Vel Leitner, N., Criquet, J., 2009. Degradation of acetic acid with sulfate radical generated by persulfate ions photolysis. Chemosphere 77, 194–200.
Kitsiou, V., Filippidis, N., Mantzavinos, D., Poulios, I., 2009. Heterogeneous and homogeneous photocatalytic degradation of the insecticide imidacloprid in aqueous solutions. Appl. Catal. B: Environ 86, 27–35.
Köck-Schulmeyer, M., Villagrasa, M., Lopez de Alda, M., Cespedes-Sanchez, R., Ventura, F., Barcelo, D., 2013. Occurrence and behavior of pesticides in wastewater treatment plants and their environmental impact. Sci. Total Environ. 458, 466–476.
Mahdi Ahmed, M., Barbati, S., Doumenq, P., Chiron, S., 2012. Sulfate radical anion oxidation of diclofenac and sulfamethoxazole for water decontamination. Chem. Eng. J. 197, 440–447.
Mahdi Ahmed, M., Chiron, S., 2014a. Ciprofloxacin oxidation by UV-C activated peroxymonosulfate in wastewater. J. Hazard. Mater. 265, 41–46.
Mahdi Ahmed, M., Chiron, S., 2014b. Solar photo-Fenton like using persulphate for carbamazepine removal from domestic wastewater. Water Res. 48, 229–236.
Neta, P., Huie, R., Ross, A., 1988. Rate constants for reactions of inorganic radicals in aqueous solution. J. Phys. Chem. Ref. Data 17, 1027–1284.
Norton-Brandao, D., Scherrenberg, S., Van Lier, J., 2013. Reclamation of used urban waters for irrigation purposes: a review of treatment technologies. J. Environ. Manage. 122, 85–98.
Olmez-Hanci, T., Arslan-Alaton, I., 2013. Comparison of sulfate and hydroxyl radical based advanced oxidation of phenol. Chem. Eng. J. 224, 10–16.
Pablos, C., Marugán, J., van Grieken, R., Serrano, E., 2013. Emerging micropollutant oxidation during disinfection processes using UV-C, UV-C/H_2O_2, UV-A/TiO_2 and UV-A/TiO_2/H_2O_2. Water Res. 47, 1237–1245.
Parry, E., Young, T., 2013. Distribution of pyrethroid insecticides in secondary wastewater effluents. Environ. Toxicol. Chem. 32, 2686–2694.
Rickman, K., Mezyk, S., 2010. Kinetics and mechanisms of sulfate radical oxidation of β-lactam antibiotics in water. Chemosphere 81, 359–365.
Ter Halle, A., Richard, C., 2006. Simulated solar light irradiation of mesotrione in natural waters. Environ. Sci. Technol. 40, 3842–3847.
Vicente, F., Santos, A., Romero, A., Rodriguez, S., 2011. Kinetic study of diuron oxidation and mineralization by persulphate: effects of temperature, oxidant concentration and iron dosage method. Chem. Eng. J. 170, 127–135.
Yuan, R., Ramjaun, S., Wang, Z., Liu, J., 2011. Effects of chloride ion on degradation of acid orange 7 by sulfate radical-based advanced oxidation process: Implications for formation of chlorinated aromatic compounds. J. Hazard. Mater. 1996, 173–179.
Zhang, T., Zhu, T., Croué, J.-P., 2013. Production of sulfate radical from peroxymonosulfate induced by a magnetically separable $CuFe_2O_4$ spinel in water: efficiency, stability, and mechanism. Environ. Sci. Technol. 47, 2784–2791.